

Benchmark Between Measured and Simulated Radiation Level Data at the Mixed-Field CHARM Facility at CERN

Daniel Prelicpean^{ID}, Giuseppe Lerner^{ID}, Rubén García Alía^{ID}, *Member, IEEE*, Kacper Bilko^{ID}, Angelo Infantino^{ID}, Diego Di Francesca^{ID}, Julia Trummer, Daniel Ricci^{ID}, Matteo Brucoli^{ID}, and Salvatore Danzeca^{ID}

Abstract—A benchmark between various radiation monitors employed at CERN for radiation to electronics applications and their simulated values with the FLUKA Monte Carlo is performed at the CHARM mixed-field irradiation facility. Comparisons are made for different operational conditions, using data recorded in the 2015–2018 period.

Index Terms—Beam loss monitor, benchmark, CERN, CERN high-energy accelerator mixed-field facility (CHARM), FLUKA, optical fiber (OF), radiation monitor, radiation to electronics (R2E).

I. INTRODUCTION

THE European Organization for Nuclear Research (CERN) hosts the CERN high-energy accelerator mixed-field facility (CHARM) [1], [2], which provides a complex mixed radiation field similar to that present in the LHC accelerator and its surroundings. Its multiple applications include the characterization of electronic devices and the calibration of radiation detectors.

The radiation environment of the CHARM facility has been studied in different contexts pertaining to radiation to electronics (R2E). Numerous tests on electronic devices have been carried out at CHARM: 1) at component level, for both cumulative effects caused by total ionizing dose (TID) [3], [4] or displacement damage (DD) [5], and stochastic effects represented by single-event effects (SEE), such as single-event latch-ups (SEL) [6]–[8] or single-event upsets (SEU) [9] and 2) at system level [10]–[13].

In addition, other dedicated analyses have been carried out for: 1) the thermalization process of secondary neu-

trons [14]; 2) the attenuation profiles of neutrons in concrete and steel [15]; and 3) activation [16].

Both the electronics tests and radiation environment measurements correspond to the 2015–2018 period, Run 2 of the Large Hadron Collider (LHC). Following the LHC schedule, the injector complex has restarted recently in view of Run 3 in 2021, and the CHARM facility is now resuming its operation as well. Of more interest for the space community is the heavy ion operation, without the use of any target, with ion species of Xe or Pb with $E > 5$ GeV/nucleon [17].

The goal of this work is to make a systematic analysis of the agreement between simulated and measured radiation levels at CHARM using a set of radiation monitors employed for R2E studies at CERN. For this purpose, the radiation levels are simulated using the FLUKA Monte Carlo code [18]–[20] (version 4.1.1) and compared to measurements performed with: 1) two beam loss monitors (BLMs) [21], [22]; 2) the RadMON system [23], [24] at different possible locations; and 3) 60 m of distributed optical fiber (OF) sensors [25]–[28], with several point dosimeters along the OF path: five RadMON RadFETs and 13 radio-photoluminescence (RPL) glass dosimeters [29], [30].

II. EXPERIMENTAL SETUP

A. CHARM Facility

While an exhaustive description of the CHARM layout, operation, and beam parameters can be found in [1], we summarize here the main features relevant for our study. The radiation field is generated by a 24-GeV proton beam, extracted from the proton synchrotron (PS) accelerator, hitting a metallic target shaped as a 50-cm-long cylinder with a diameter of 8 cm, and it is used to test electronic components and systems at predefined test positions (see Fig. 1) within the irradiation room of $7 \times 5 \times 2$ m³. Therefore, CHARM is a spallation source, similar to well-known atmospheric-like neutron irradiation facilities, such as TRIUMF [31], LANSCE [32] or ChipIr [33]. The similarity between CHARM and these facilities is the ability to reproduce radiation fields of interest (for CHARM, the accelerator environment) that can be used to irradiate devices under test (DUTs), while the two main

Manuscript received 8 January 2022; revised 6 February 2022; accepted 17 April 2022. Date of publication 25 April 2022; date of current version 18 July 2022.

Daniel Prelicpean is with the European Organization for Nuclear Research, 1211 Geneva, Switzerland, and also with the Department of Physics, Technical University of Munich, 80333 Munich, Germany (e-mail: daniel.prelicpean@cern.ch).

Giuseppe Lerner, Rubén García Alía, Kacper Bilko, Angelo Infantino, Diego Di Francesca, Julia Trummer, Daniel Ricci, Matteo Brucoli, and Salvatore Danzeca are with the European Organization for Nuclear Research, 1211 Geneva, Switzerland.

Color versions of one or more figures in this article are available at <https://doi.org/10.1109/TNS.2022.3169756>.

Digital Object Identifier 10.1109/TNS.2022.3169756

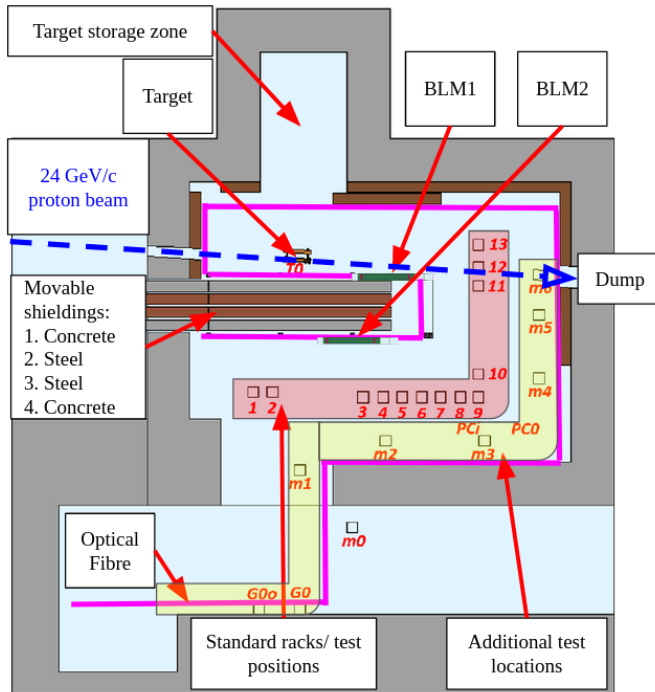


Fig. 1. Top view of FLUKA geometry of the CHARM test area. Two BLMs are installed at 1 m above beam height, one next to the target and one behind the movable shieldings. There are 13 racks (standard test locations) at beam height where RadMONs can be deployed, with additional positions distributed in the test area. An OF duct was mounted along the walls and the movable shieldings.

differences are: 1) the much larger initial proton energy in CHARM and 2) the fact that the secondary radiation field is composed of both neutrons and charged particles (and therefore is a mixed field) and covers the full irradiation room. Different target and shielding configurations are available in order to produce a secondary field with a broad range of radiation intensities, compositions, and spectra.

- 1) *Target Material (in Decreasing Density)*: Copper (Cu), aluminum (Al), and sieved aluminum/aluminum with holes (Al_h) can be used. The lower the target material density is, the lower the secondary field intensity becomes.
- 2) *Shielding Configuration*: Movable blocks with dimensions of 20/214/350 cm (width/height/length) and made of concrete or stainless steel can be placed between the target and the test locations in different combinations (see Fig. 1).

The configurations of the movable shieldings are labeled using four consecutive letters, the first corresponding to the closest block to the target. For each block, the operational usages are: no shielding (O), concrete (C), or stainless steel (S). The several possible configurations (e.g., copper with full shielding, CuCSSC) allow to modulate the radiation field according to the specific user needs.

The provided values at CHARM are normalized to the protons on target (POT), which are measured using dedicated beam instrumentation devices called secondary emission chambers (XSECs) [34], relying on the phenomenon of secondary electron emission from the surfaces of thin metal foils

TABLE I

MAXIMUM AND WEEKLY MAXIMUM INTEGRATED RATES AT CHARM FOR THE TID, AND THE THERMAL NEUTRON EQUIVALENT AND HIGH-ENERGY HADRON FLUENCES, OBTAINED AT THE R10 LOCATION BASED ON FLUKA SIMULATIONS

Quantity	Maximum Rate	Integrated Rate (per week)
Total Ionizing Dose	2.70 Gy/h	360 Gy
Thermal neutron fluence	$3 \times 10^6 \text{ cm}^{-2}\text{s}^{-1}$	$1.5 \times 10^{12} \text{ cm}^{-2}$
High-energy hadron fluence	$1.5 \times 10^6 \text{ cm}^{-2}\text{s}^{-1}$	$8 \times 10^{11} \text{ cm}^{-2}$

hit by charged particles. The secondary electrons collected by high-voltage electrodes are directly proportional to the total number of incoming particles.

Typical POT figures at CHARM are of approximately 5×10^{11} protons/spill and 1.5×10^{16} protons/week. The time structure of the proton beam impinging the target, and hence of the mixed-field environment, is that of a quasi-uniform spill lasting roughly 350 ms, which is repeated every 10 s. Although this would indeed be a pulsed beam for TID purposes, for SEE testing, it can still be considered as a quasi-continuous beam, given that the spill duration is orders of magnitude longer than characteristic SEE induction times (tens of nanoseconds).

The maximum dose rates and fluxes achievable in the standard CHARM test locations, considering a typical week of operation (5.5 days of actual irradiation, with 0.25-day access and 1.25-day cool-down before access), can be seen in Table I. The maximum is considered based on FLUKA simulations for the CuOOOO configuration at the R10 rack location, as it is closest to the beam, without actually being placed in the beam or the beam halo, such as R11, R12, R13, and m0.

B. FLUKA Simulation

The radiation environment of the CHARM facility is simulated using the previously introduced Monte Carlo code FLUKA, capable of calculating R2E-relevant quantities. A full model of the experimental setup is implemented (see Figs. 1 and 2, where the latter includes also a simulated 2-D map of TID at beam height for two different configurations, CuOOOO and CuCSSC). Compared to the simulation model previously used in [1], the explicit modeling of two-beam loss monitors (see Section III-A) and the OF (see Section III-B) is included. Moreover, the concrete density (relevant for thermalization of neutrons) and the shielding material are updated to the latest estimations and measurements to be as realistic as possible, but not necessarily yielding a better agreement.

The FLUKA settings used for the simulations are the following: NEW-DEFA DEFAULTS, energy thresholds for both transport and production of all particles at 100 keV (excluding neutrons that are simulated down to 10^{-5} eV). Regarding the thermalization of neutrons, their transport at energies lower than 20 MeV is performed in FLUKA via a multigroup algorithm, where neutrons are grouped in 260 groups. For energies larger than 20 MeV, elastic and inelastic reactions are simulated as exclusive processes and below on a group-to-group basis as transfer probabilities forming a so-called downscattering matrix. The simulated particle spectra have

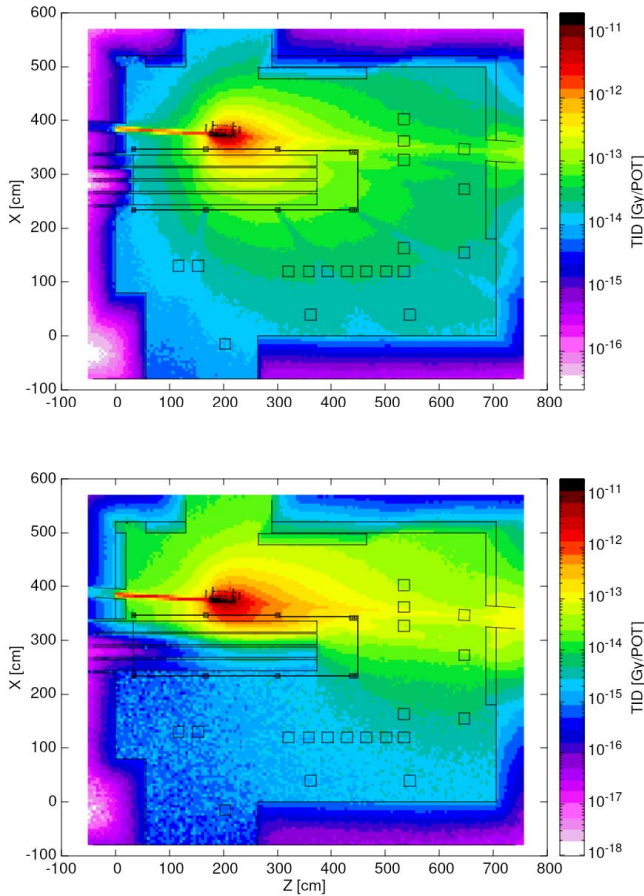


Fig. 2. Simulated 2-D TID distribution at beam height is shown for two configurations: CuOOOO (top) and CuCSSC (bottom).

been recorded at all test locations, with two examples given in Fig. 3.

C. Comparison Between CHARM and the Accelerator Environment at the LHC

The radiation environment of the LHC is well reproduced at CHARM, as previously hinted in [1] for the case of the LHC shielded alcoves hosting electronics. The main difference is the presence of the very high-energy (>24 GeV) particles at the LHC. The similarity is further confirmed in our study by comparing the normalized distributions of the particle energy spectra in the BLMs at the LHC (installed on the accelerator in the tunnel) and at CHARM, as shown in Fig. 4 for the proton and neutron energy comparisons.

III. BENCHMARK RESULTS

This section presents the results of the comparison between FLUKA simulations and data of radiation monitors, normalized to the number of primary protons on target (POT).

A. Beam Loss Monitors

The BLM system [35], [36] has been developed at CERN, in particular at the LHC, in order to protect the machine

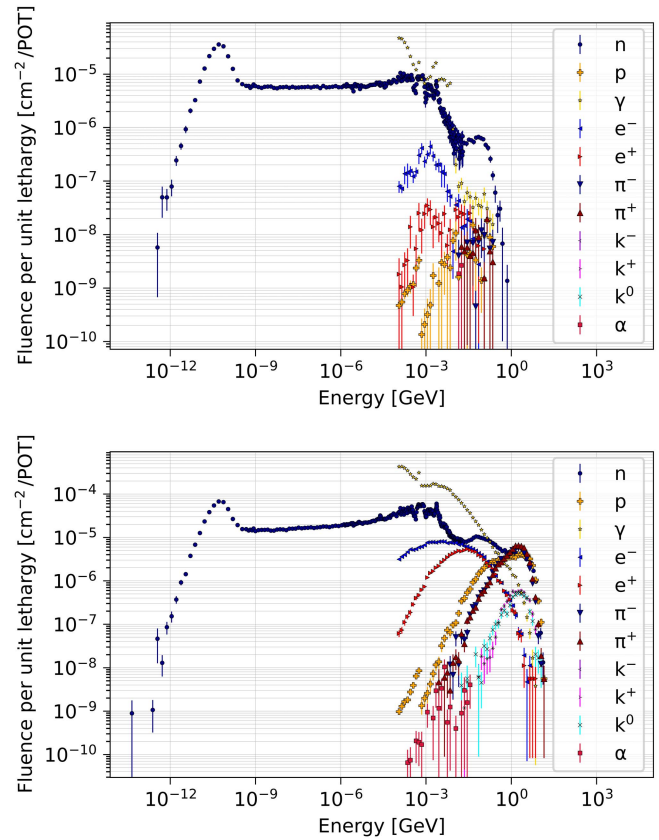


Fig. 3. Particle spectrum scored at the standard test locations for the CuCSSC configuration: R1, fully shielded (top), and R13, within the residual beam direction (bottom), in a lethargy format.

components from damage, for example, to prevent the superconducting magnets from quenching in case of unexpected beam losses. The LHC is equipped with approximately 4000 BLMs that detect fast beam losses and can trigger the beam dump mechanism in case the signal exceeds predefined thresholds.

As anticipated, the CHARM experimental area includes two-BLMs that measure the absorbed dose (in Gy), installed at 1 m above beam height, one next to the target and one behind the movable shieldings (see Fig. 1). Although there are multiple BLM types at CERN, the most common one (also used at CHARM) is the ionization chamber (IC), shaped as a cylinder, approximately 48 cm long with an inner radius of 4.25 cm, yielding a nominal active volume of N_2 at 100-mbar overpressure of 1.5 L. Ionizing particles traversing the sensitive volume produce electron-ion pairs, which are collected at the anode and cathode by applying high voltages (up to several kilovolts) between them.

While at the CHARM facility, the radiation shower originates from the beam colliding with a target, at the LHC, the beam particles are lost around the accelerator and initiate hadronic showers through elements along the beamline (such as magnets or absorbers), which are then measured by the BLMs usually installed in the shower peak outside the element.

A comparison between BLM TID measurements and simulations at CHARM, obtained with full modeling of the BLMs

TABLE II

SUMMARY OF MEASURED AND SIMULATED BLM TID VALUES, AS WELL AS THEIR RATIOS, FOR THE THREE TARGETS: COPPER (Cu), ALUMINUM (al) AND ALUMINUM WITH HOLES (Al_h), AND THE USED SHIELDING CONFIGURATIONS (CONF.). THE NUMBER OF PROTON ON TARGET (POT) IS AN INDICATOR OF HOW MUCH (IN ABSOLUTE TERMS) THE RESPECTIVE CONFIGURATION HAS BEEN USED: CUOOOO WAS THE MOST USED CONFIGURATION FOR THE HIGH INTENSITY, AND CUCSSC AND Al_h CSSC WERE THE MOST USED CONFIGURATION FOR LOW INTENSITIES. THE LAST ROW OF EACH TABLE PRESENTS THE AVERAGE RATIO OF THE MEASURED TO SIMULATED VALUES AND THEIR STANDARD DEVIATION. (a) COPPER TARGET. (b) ALUMINUM TARGET. (c) ALUMINUM WITH HOLES TARGET

(a)

CONF.	POT	BLM1			BLM2			BLM1/2 ratio		
		measured [Gy/POT]	simulated [Gy/POT]	measured/simulated	measured [Gy/POT]	simulated [Gy/POT]	measured/simulated	measured	simulated	measured/simulated
CuOOOO	$3.14 \times 10^{+17}$	4.74×10^{-14}	5.33×10^{-14}	0.89	2.39×10^{-14}	3.22×10^{-14}	0.74	1.98	1.66	1.20
CuOOOC	$4.53 \times 10^{+13}$	5.86×10^{-14}	5.34×10^{-14}	1.10	2.01×10^{-14}	3.36×10^{-14}	0.60	2.92	1.59	1.84
CuCOOO	$3.21 \times 10^{+13}$	5.96×10^{-14}	5.64×10^{-14}	1.06	1.21×10^{-14}	1.10×10^{-14}	1.10	4.93	5.14	0.96
CuOOSC	$1.73 \times 10^{+13}$	5.92×10^{-14}	5.49×10^{-14}	1.08	4.27×10^{-15}	5.52×10^{-15}	0.77	13.86	9.95	1.39
CuCSOO	$8.46 \times 10^{+14}$	5.06×10^{-14}	5.66×10^{-14}	0.89	2.32×10^{-15}	3.13×10^{-15}	0.74	21.81	18.09	1.21
CuOSSC	$1.83 \times 10^{+13}$	5.97×10^{-14}	5.58×10^{-14}	1.07	2.67×10^{-15}	2.87×10^{-15}	0.93	22.36	19.45	1.15
CuCSSO	$9.00 \times 10^{+14}$	5.99×10^{-14}	5.76×10^{-14}	1.04	2.03×10^{-15}	2.44×10^{-15}	0.83	29.51	23.62	1.25
CuCSSC	$2.46 \times 10^{+16}$	5.20×10^{-14}	5.80×10^{-14}	0.90	1.71×10^{-15}	2.99×10^{-15}	0.57	30.41	19.37	1.57
AVG				1.00±0.09			0.79±0.17			1.32±0.27

(b)

CONF.	POT	BLM1			BLM2			BLM1/2 ratio		
		measured [Gy/POT]	simulated [Gy/POT]	measured/simulated	measured [Gy/POT]	simulated [Gy/POT]	measured/simulated	measured	simulated	measured/simulated
AIOOOO	$2.18 \times 10^{+14}$	3.93×10^{-14}	3.62×10^{-14}	1.09	1.34×10^{-14}	1.35×10^{-14}	0.99	2.93	2.68	1.09
AICSOO	$3.41 \times 10^{+14}$	4.20×10^{-14}	3.89×10^{-14}	1.08	1.39×10^{-15}	1.79×10^{-15}	0.78	30.22	21.72	1.39
AICSSC	$5.19 \times 10^{+14}$	4.19×10^{-14}	3.85×10^{-14}	1.09	9.62×10^{-16}	1.41×10^{-15}	0.68	43.56	27.28	1.60
AVG				1.08±0.01			0.82±0.16			1.36±0.25

(c)

CONF.	POT	BLM1			BLM2			BLM1/2 ratio		
		measured [Gy/POT]	simulated [Gy/POT]	measured/simulated	measured [Gy/POT]	simulated [Gy/POT]	measured/simulated	measured	simulated	measured/simulated
Al_h OOOO	$6.25 \times 10^{+14}$	1.35×10^{-14}	2.00×10^{-14}	0.67	4.63×10^{-15}	8.05×10^{-15}	0.57	2.92	2.49	1.17
Al_h COOO	$1.12 \times 10^{+13}$	1.46×10^{-14}	2.09×10^{-14}	0.70	2.49×10^{-15}	3.74×10^{-15}	0.67	5.86	5.59	1.05
Al_h CSOO	$2.83 \times 10^{+13}$	1.45×10^{-14}	2.11×10^{-14}	0.69	5.34×10^{-16}	1.06×10^{-15}	0.50	27.15	19.85	1.37
Al_h CSSO	$3.03 \times 10^{+14}$	1.42×10^{-14}	2.09×10^{-14}	0.68	4.27×10^{-16}	7.19×10^{-16}	0.59	33.26	29.15	1.14
Al_h CSSC	$9.95 \times 10^{+15}$	1.40×10^{-14}	2.12×10^{-14}	0.66	3.92×10^{-16}	6.59×10^{-16}	0.59	35.71	32.14	1.11
AVG				0.68±0.01			0.59±0.06			1.17±0.12

in the FLUKA geometry, is presented in Table II, showing separately the two BLMs. The results exhibit a satisfactory level of agreement, always within 50%, and often much better for individual configurations. For the case of the copper (Cu) target, the average ratio of the measured values over FLUKA simulated ones is of 1.00 ± 0.09 (the error given is the standard deviation) for the highly irradiated BLM1, 0.79 ± 0.17 for the more shielded BLM2. For the sieved aluminum (Al_h) target, a systematic shift seems to be present, which shall be further investigated. The only difference is the target, consisting of half the material compared to the aluminum one, yielding lower radiation levels that are more sensitive to geometry mismodelings. From Table II(b), the agreement

for the shielded BLM2 decreases with the dose, supporting this hypothesis.

B. Optical Fiber Dosimetry

The OF dosimeter presents the advantage of measuring spatially distributed TID profiles, compared to the point-like measurements of BLMs or RadMONs. The results of TID measurements with an OF dosimeter have been previously presented in [28], together with a first comparison with FLUKA predictions, and a similar benchmark with the updated simulation is included in this work.

The OF dosimeter of only $125 \mu\text{m}$ in diameter is too small (compared to the $7 \times 5 \times 2 \text{ m}^3$ CHARM irradiation room) to be

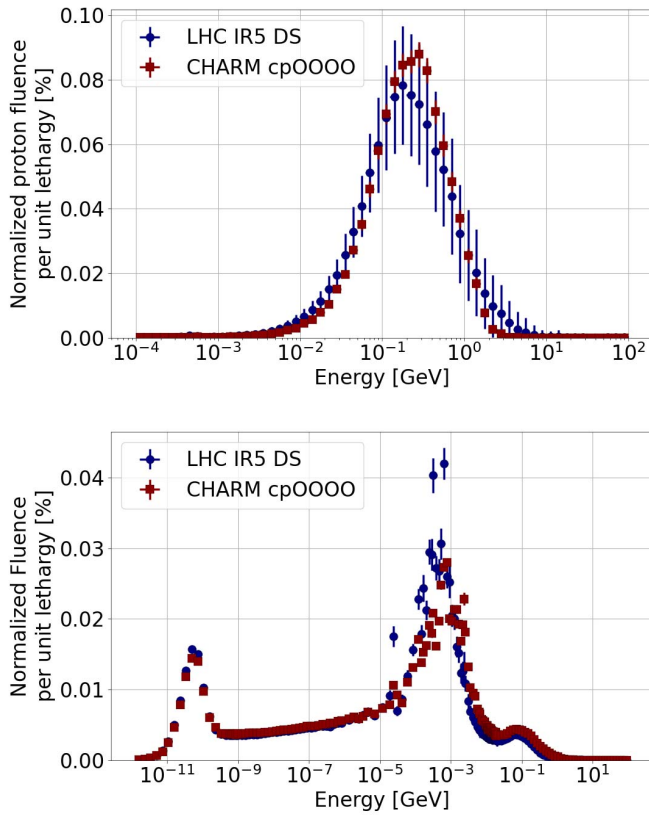


Fig. 4. Comparison of the FLUKA-simulated particle spectrum scored in the active volume of the BLMs between CHARM and LHC IP5 for protons (top) and neutrons (bottom), in a lethargy format. The larger error bars on the LHC simulation are due to the more complex and significantly larger geometry.

included as an exact replica in the FLUKA geometry because there will not be sufficiently many particles reaching the OF regions. To improve the CPU efficiency, the OF is modeled as a cylinder made of SiO_2 with a radius of 1 cm, to balance the build-up (mainly for photons) and self-shielding effects of the radiation penetrating matter. This geometric improvement represents a significant update with respect to the FLUKA simulation used in [28], where scoring of dose in air was used.

The path of the OF cable (schematically shown in Fig. 1) follows the walls of the facility, with regions close to the target where peaks are observed in Fig. 5 at 60 and 75 m. The OF segment between (65, 70) m is mounted behind the movable shieldings, causing the pronounced decrease in the estimated levels for the fully shielded configuration.

The shape of the 1-D profile is very well reproduced (see Fig. 5), and the ratio of measured and simulated dose is generally well within the 50% margin, with local fluctuations in both directions. The average (weighted on TID) of the measured over simulation ratio is 0.93 ± 0.24 for the CuO000 shielding and 0.99 ± 0.32 for the CuCSSC shielding.

Moreover, for the CuO000 configuration, point-wise measurements were recorded by five RadMON RADFETS and thirteen RPLs, which were placed along the OF path around the radiation peak. Their averaged measured to simulated dose ratio is of 1.05 ± 0.39 for the RadMON RADFETS and 0.80 ± 0.27 for the RPLs, which are considered to be good.

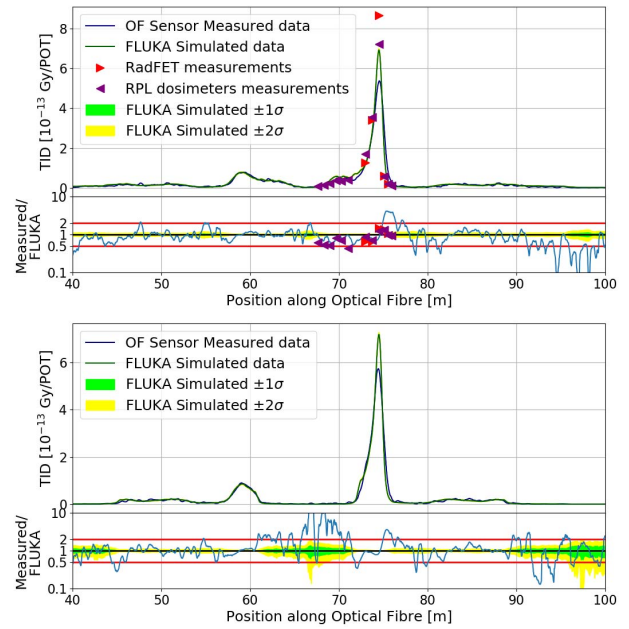


Fig. 5. OF benchmark for two shielding configurations: CuCSSC (bottom) and CuO000 (top), for which additional point-wise RadFET and RPL monitors could be installed. The green and yellow bands are the $\pm 1\sigma$ and $\pm 2\sigma$ simulated statistical uncertainty intervals, respectively, centered on the FLUKA simulation result. The lower pad in each plot shows the ratio between the measurements and simulation. Red lines display the 50% discrepancy range.

C. Radiation Monitors

The CHARM facility includes a set of RadMON detectors measuring key R2E-relevant quantities, including: 1) TID; 2) HEH-eq fluence, i.e., fluence of $E > 20$ -MeV hadrons plus an “equivalent contribution of intermediate-energy (0.2–20 MeV) neutrons with energy-dependent Weibull weights; and 3) thermal neutron equivalent fluence, where neutrons are weighted proportionally to the inverse of their velocity [37].

1) *Fluence Results*: The above fluences are calculated in FLUKA in $20 \times 20 \times 20 \text{ cm}^3$ air volumes in the positions of interest without explicitly modeling the geometry of the RadMON detectors, unlike the case of the BLMs: this choice is motivated by the small size of the RadMON and by the fact that, compared to the TID, the hadron fluences are expected to be less dependent on the material and detector geometry.

Depending on the location (see Fig. 1), the RadMONs (or in normal operation, the test equipment) are exposed to a radiation field with different compositions and particle energy spectra. In positions closer to the beam, the field contains a large amount of charged hadrons with particle energies extending up to the giga-electronvolt range. In positions perpendicular to the target, the environment contains a relatively larger amount of neutrons, which span until lower energies than charged hadrons. When the shielded configuration is employed, the relative amount of thermal neutrons is further enhanced.

The results of the benchmarking between RadMON measurements and simulations are presented in Table III for the CuO000 CHARM configuration. One consistent feature

TABLE III

RADMON BENCHMARK RESULTS FOR THE CUOOOO CONFIGURATION. NOTE THAT RADMONS HAVE NOT BEEN EMPLOYED AT ALL POSSIBLE TEST LOCATIONS; NEVERTHELESS, FLUKA ALLOWS FOR ESTIMATING THE DESIRED SET OF R2E QUANTITIES

LOC.	High Energy Hadrons			Thermal Neutrons			R-FACTOR		
	measured [cm ⁻² /POT]	simulated [cm ⁻² /POT]	measured/ simulated	measured [cm ⁻² /POT]	simulated [cm ⁻² /POT]	measured/ simulated	measured [cm ⁻² /POT]	simulated [cm ⁻² /POT]	measured/ simulated
R1	1.85×10 ⁻⁵	3.47×10 ⁻⁵	0.53	5.48×10 ⁻⁵	1.20×10 ⁻⁴	0.46	2.44	5.91	0.41
R4	4.28×10 ⁻⁵	5.13×10 ⁻⁵	0.83	3.90×10 ⁻⁵	1.26×10 ⁻⁴	0.31	0.91	3.29	0.28
R5	3.49×10 ⁻⁵	4.40×10 ⁻⁵	0.79	4.60×10 ⁻⁵	1.27×10 ⁻⁴	0.36	1.32	3.78	0.35
R7	4.32×10 ⁻⁵	4.72×10 ⁻⁵	0.92	4.43×10 ⁻⁵	1.26×10 ⁻⁴	0.35	1.03	3.37	0.31
R9	2.96×10 ⁻⁵	4.35×10 ⁻⁵	0.68	5.86×10 ⁻⁵	1.24×10 ⁻⁴	0.47	1.98	3.54	0.56
R10	3.28×10 ⁻⁵	5.18×10 ⁻⁵	0.63	5.74×10 ⁻⁵	1.23×10 ⁻⁴	0.47	1.75	2.84	0.62
R13	6.66×10 ⁻⁵	8.32×10 ⁻⁵	0.80	5.98×10 ⁻⁵	1.16×10 ⁻⁴	0.51	0.90	1.55	0.58
m2	3.39×10 ⁻⁵	3.29×10 ⁻⁵	1.03	1.32×10 ⁻⁴	1.32×10 ⁻⁴	1.00	3.89	4.01	0.97
AVG.			0.86±0.18			0.49±0.22			0.47±0.15

TABLE IV

COMPARISON OF RADMON (RADFET) TID DATA WITH FLUKA RESULTS FOR THE COPPER TARGET WITHOUT AND WITH SHIELDINGS, CONSIDERING BOTH THE STANDARD CHARM SIMULATION AND THE SECOND STEP APPROACH. (a) COPPER TARGET, NO SHIELDING (CUOOOO) CONFIGURATION. (b) COPPER TARGET, WITH SHIELDING (CUSSO) CONFIGURATION

(a)

LOC.	Measured TID [Gy/POT]	Simulated 1-step [Gy/POT]	Measured/ Simulated 1-step	Simulated 2-step [Gy/POT]	Measured/ Simulated 2-step	Simulated 2-step/ -step
G0	2.50×10 ⁻¹⁵	2.97×10 ⁻¹⁵	0.84	3.08×10 ⁻¹⁵	0.81	1.04
R1	1.20×10 ⁻¹⁴	1.40×10 ⁻¹⁴	0.86	1.21×10 ⁻¹⁴	0.99	0.86
R4	2.17×10 ⁻¹⁴	2.58×10 ⁻¹⁴	0.84	2.85×10 ⁻¹⁴	0.76	1.11
R5	1.70×10 ⁻¹⁴	2.10×10 ⁻¹⁴	0.81	2.00×10 ⁻¹⁴	0.85	0.95
R7	1.95×10 ⁻¹⁴	2.51×10 ⁻¹⁴	0.78	3.14×10 ⁻¹⁴	0.62	1.25
R9	1.70×10 ⁻¹⁴	2.34×10 ⁻¹⁴	0.73	2.32×10 ⁻¹⁴	0.73	1.00
R10	2.41×10 ⁻¹⁴	2.61×10 ⁻¹⁴	0.92	2.49×10 ⁻¹⁴	0.97	0.95
R13	3.00×10 ⁻¹⁴	3.86×10 ⁻¹⁴	0.78	3.88×10 ⁻¹⁴	0.77	1.00
m6	1.49×10 ⁻¹³	7.86×10 ⁻¹⁴	1.90	8.86×10 ⁻¹⁴	1.68	1.13
m2	1.41×10 ⁻¹⁴	1.70×10 ⁻¹⁴	0.83	1.53×10 ⁻¹⁴	0.92	0.90
AVG			0.93±0.34		0.91±0.29	1.02±0.12

(b)

LOC.	Measured TID [Gy/POT]	Simulated [Gy/POT]	Measured/ Simulated	Simulated 2nd step [Gy/POT]	Measured/ Simulated 2nd step	Simulated 2nd step/ 1st step
R1	7.28×10 ⁻¹⁶	1.05×10 ⁻¹⁵	0.69	6.79×10 ⁻¹⁶	1.07	0.65
R4	1.48×10 ⁻¹⁵	1.87×10 ⁻¹⁵	0.79	1.17×10 ⁻¹⁵	1.27	0.63
R7	2.16×10 ⁻¹⁵	2.57×10 ⁻¹⁵	0.84	1.87×10 ⁻¹⁵	1.16	0.73
R10	2.44×10 ⁻¹⁵	4.34×10 ⁻¹⁵	0.56	3.39×10 ⁻¹⁵	0.72	0.78
m2	1.77×10 ⁻¹⁵	2.26×10 ⁻¹⁵	0.78	1.25×10 ⁻¹⁵	1.41	0.55
AVG			0.73±0.11		1.13±0.26	0.67±0.09

(also for other configurations) is that for HEHeq fluence, the agreement is satisfactory, with an average measured/simulated ratio of 0.78 ± 0.16 (i.e., an overestimation by 22%), whereas for thermal-energy neutrons, this decreases to 0.49 ± 0.22 and, for the R-Factor, this decreases to 0.47 ± 0.15 (i.e., an overestimation by a factor 2). Globally, these results exhibit a satisfactory level of agreement within a factor of 2, common in mixed-field benchmark-related studies. The difficulty of accurately simulating the thermal neutron environment is mainly considered to arise from the uncertainties in the exact material composition, density, and uniformity (especially of the concrete walls, despite the best efforts to assess them). The better agreement at the m2 location compared to other locations is present not only for the CuOOOO configuration but for the others as well; however, it is the location closest

to the walls, thereby also most susceptible to systematic uncertainties in material mismodelings.

2) *TID Results With Two-Step Simulation Approach*: Since the RadMON detectors are not explicitly modeled due to their small size, the TID (as energy deposition per unit mass) was evaluated in air in the $20 \times 20 \times 20$ cm³ volume. However, such a procedure has several limitations. The most notable example is the ¹⁴N(n,p)¹⁴C reaction of thermal neutrons leading to an overestimation of the deposited dose in air [38]: the resulting 590-keV proton will deposit its energy through ionization processes [39].

One solution would be to set a high neutron energy cutoff at 1 MeV to suppress most of the ¹⁴N(n,p)¹⁴C reactions, as previously performed in [28]. However, in order not to fully neglect the neutron TID contribution below 1 MeV,

an alternative second step simulation has been studied in [40], where the particle fluences obtained from initial simulation are used as the new source/beam that hits an explicit model of the detectors, in this case the RadMON RADFET. The beam is modeled as a wide uniform beam as large as the irradiated detector, assuming a mono-directional radiation source. Considering that most of the radiation comes from the CHARM target, this is a reasonable approximation. The second step uses the suggested simulation settings mentioned in [40], namely: 1) a RADFET oxide with 400 nm thickness; 2) PRECISIO default settings in FLUKA; 3) particle transport thresholds set at 1 keV; and 4) input spectra cutoff at 100 keV (for all particles, except neutrons), in order to speed up the simulation, as particles with energy lower than 100 keV usually do not penetrate the RadFET lid (box) and do not contribute to the deposited dose [40].

Both the results of the direct simulation and the second step, together with the measured value and their ratios, are presented for each available rack location in Table IV for the CuOOOO and CuCSSO configurations. The last row presents the average ratio of the measured to simulated values over all locations. While some configurations show a negligible difference (e.g. CuOOOO), other configurations (especially the shielded ones, e.g., CuCSSO) exhibit an improvement in the agreement level.

The study carried out in [40] considered only the R1 location for the CuOOOO configuration only, as it was meant to be an exploratory study to find the most suitable simulation parameters. Taking advantage of this, these results extend to a wider range of configurations (available upon request) and locations in order to study the usefulness of the second step approach. The 20% improvement indicated in [40] in the simulated dose is supported by our results, in particular for the shielded configurations, where the radiation field contains more neutrons that contribute to the $^{14}\text{N}(n,p)^{14}\text{C}$ reaction.

Such a two-step simulation procedure could yield improved results also in specific locations where the radiation field is composed predominantly of neutrons and where computational statistics are sufficiently good.

IV. CONCLUSION AND DISCUSSION

This work presented a comprehensive benchmarking of FLUKA simulations and radiation-level measurements from different detectors in the CHARM facility at CERN. Numerically, the agreement between the measured values of the radiation monitors employed at CHARM and their FLUKA simulated values is generally good (on average around $\pm 20\%$) for BLMs, OF sensors, RPL glass dosimeters, and radiation monitors (RadMON) measurements of the TID and high-energy hadron (HEH-eq) fluence, while an overestimation by approximately a factor of 2 is observed in the case of RadMON thermal neutron (THN) fluence measurements. This study represents the first systematic benchmark at CHARM, and however, there are similar BLM benchmarks at the LHC [36] that result in varying average levels of agreement (from 10% to 40% to a factor of 3, depending on the source of radiation and location).

This article showcases the importance of Monte Carlo radiation environment simulations to better understand the radiation field composition, including 3-D spatial resolution, particle energy spectra for mixed-field constituents, and the capacity of characterizing future operational scenarios and machines, among other applications. By benchmarking the simulations against measurements, we aim to confirm the accuracy of the simulation models of the facility and the use cases of the radiation monitors.

These results demonstrate that the complex mixed-field radiation environment of CHARM is well controlled and understood due to the many different radiation monitors that are employed and can hence be used reliably for the qualification of electronic equipment.

AUTHOR CONTRIBUTION

The authors of this article are members of CERN. D. Prelipcean and G. Lerner wrote this article, with input from R. G. Alía. D. Prelipcean ran the FLUKA simulations and extracted the estimated radiation monitors data thereof. A. Infantino provided input in updating the CHARM FLUKA model. K. Bilko provided the BLM data, D. D. Francesca and D. Ricci provided the OF data, J. Trummer provided the RPL data, and M. Brucoli and S. Danzeca provided the RadMON data. All authors contributed to the work and approved the submitted version.

REFERENCES

- [1] J. Mekki, M. Brugger, R. G. Alia, A. Thornton, N. C. D. S. Mota, and S. Danzeca, "CHARM: A mixed field facility at CERN for radiation tests in ground, atmospheric, space and accelerator representative environments," *IEEE Trans. Nucl. Sci.*, vol. 63, no. 4, pp. 2016–2114, Aug. 2016.
- [2] A. Infantino *et al.*, "Dose gradient assessment at the new cern charm irradiation facility," *Radiat. Phys. Chem.*, vol. 155, pp. 225–232, Feb. 2019.
- [3] R. Ferraro *et al.*, "Study of the impact of the LHC radiation environments on the synergistic displacement damage and ionizing dose effect on electronic components," *IEEE Trans. Nucl. Sci.*, vol. 66, no. 7, pp. 1548–1556, Jul. 2019.
- [4] C. Cazzaniga, R. G. Alia, M. Kastriotou, M. Cecchetto, P. Fernandez-Martinez, and C. D. Frost, "Study of the deposited energy spectra in silicon by high-energy neutron and mixed fields," *IEEE Trans. Nucl. Sci.*, vol. 67, no. 1, pp. 175–180, Jan. 2020.
- [5] R. Ferraro *et al.*, "COTS optocoupler radiation qualification process for LHC applications based on mixed-field irradiations," *IEEE Trans. Nucl. Sci.*, vol. 67, no. 7, pp. 1395–1403, Jul. 2020.
- [6] M. Cecchetto *et al.*, "SEE flux and spectral hardness calibration of neutron spallation and mixed-field facilities," *IEEE Trans. Nucl. Sci.*, vol. 66, no. 7, pp. 1532–1540, Jul. 2019.
- [7] R. G. Alia *et al.*, "SEL hardness assurance in a mixed radiation field," *IEEE Trans. Nucl. Sci.*, vol. 62, no. 6, pp. 2555–2562, Dec. 2015.
- [8] N. Kerboub *et al.*, "Comparison between in-flight SEL measurement and ground estimation using different facilities," *IEEE Trans. Nucl. Sci.*, vol. 66, no. 7, pp. 1541–1547, Jul. 2019.
- [9] G. Tsiligianis *et al.*, "Radiation effects on deep submicrometer SRAM-based FPGAs under the CERN mixed-field radiation environment," *IEEE Trans. Nucl. Sci.*, vol. 65, no. 8, pp. 1511–1518, Aug. 2018.
- [10] A. Coronetti *et al.*, "Radiation hardness assurance through system-level testing: Risk acceptance, facility requirements, test methodology, and data exploitation," *IEEE Trans. Nucl. Sci.*, vol. 68, no. 5, pp. 958–969, May 2021.
- [11] A. Coronetti *et al.*, "Mixed-field radiation qualification of a COTS space on-board computer along with its CMOS camera payload," in *Proc. RADECS Conf.*, Sep. 2019, vol. 68, no. 5, pp. 958–969.
- [12] J. Budroweit *et al.*, "In-situ testing of a multi-band software-defined radio platform in a mixed-field irradiation environment," *Aerospace*, vol. 6, no. 10, p. 106, Sep. 2019.

- [13] R. Secondo *et al.*, "System level radiation characterization of a 1U CubeSat based on CERN radiation monitoring technology," *IEEE Trans. Nucl. Sci.* vol. 65, no. 8, pp. 1694–1699, Aug. 2018.
- [14] T. Oyama *et al.*, "Measurement and calculation of thermal neutrons induced by the 24 GeV/c proton bombardment of a thick copper target," *Nucl. Instrum. Methods Phys. Res. B, Beam Interact. Mater. At.*, vol. 434, pp. 29–36, Nov. 2018.
- [15] E. Lee *et al.*, "Energy spectra of neutrons penetrating concrete and steel shielding blocks from 24 GeV/c protons incident on thick copper target," *Nucl. Instrum. Methods Phys. Res. Sect. A: Accel., Spectrometers, Detectors Associated Equip.*, vol. 998, May 2021, Art no. 165189.
- [16] T. Oyama *et al.*, "Measurements of secondary-particle emissions from copper target bombarded with 24-GeV/c protons," *Nucl. Instrum. Methods Phys. Res. A, Accel. Spectrom. Detect. Assoc. Equip.*, vol. 990, Feb. 2021, Art no. 164977.
- [17] P. Fernández-Martánez *et al.*, "SEE tests with ultra energetic Xe ion beam in the CHARM facility at CERN," *IEEE Trans. Nucl. Sci.*, vol. 66, no. 7, pp. 1523–1531, Jul. 2019.
- [18] (Jun. 4, 2021). *FLUKA*. [Online]. Available: <https://fluka.cern>
- [19] G. Battistoni *et al.*, "Overview of the FLUKA code," *Annals Nucl. Energy*, vol. 82, pp. 10–18, Aug. 2015.
- [20] T. T. Böhlen *et al.*, "The FLUKA code: Developments and challenges for high energy and medical applications," *Nucl. Data Sheets*, vol. 120, pp. 211–214, Jun. 2014.
- [21] E. Holzer *et al.*, "Beam loss monitoring system for the LHC," in *Proc. IEEE Nucl. Sci. Symp. Conf. Rec.*, vol. 2, Oct. 2005, pp. 1052–1056.
- [22] V. Grishin *et al.*, "A family of gas ionization chambers and SEM for beam loss monitoring of LHC and other accelerators," in *Proc. 26th Russian Part. Accel. Conf. (RuPAC)*, Nov. 2018, pp. 44–48.
- [23] G. Spiezia *et al.*, "A new RadMon version for the LHC and its injection lines," *IEEE Trans. Nucl. Sci.*, vol. 61, no. 6, pp. 3424–3431, Dec. 2014.
- [24] S. Danzeca, "The new version of the radiation monitor system for the electronics at the CERN: Electronic components radiation hardness assurance and sensors qualification," Ph.D. dissertation, Doctoral School Inf., Struct. Syst., Université Montpellier, Montpellier, France, Apr. 2015.
- [25] D. D. Francesca *et al.*, "Qualification and calibration of single-mode phosphosilicate optical fiber for dosimetry at CERN," *J. Lightw. Technol.*, vol. 37, no. 18, pp. 4643–4649, Sep. 15, 2019.
- [26] G. Li Vecchi *et al.*, "Distributed optical fiber radiation sensing at CERN," in *Proc. 9th Int. Part. Accel. Conf.*, Apr. 2018, p. 4.
- [27] D. Di Francesca *et al.*, "Implementation of optical fiber based dosimetry at CERN," in *Proc. 26th Int. Conf. Opt. Fiber Sensors*, Sep. 2018, p. WC1.
- [28] D. Di Francesca *et al.*, "Dosimetry mapping of mixed-field radiation environment through combined distributed optical fiber sensing and FLUKA simulation," *IEEE Trans. Nucl. Sci.*, vol. 66, no. 1, pp. 299–305, Jan. 2019.
- [29] H. Schönbacher *et al.*, "High-level dosimetric methods," *Radiat. Protection Dosimetry*, vol. 137, pp. 83–93, Sep. 2009.
- [30] H. Vincke *et al.*, "Response of alanine and radio-photo-luminescence dosimeters to mixed high-energy radiation fields," *Radiat. Protection Dosimetry*, vol. 125, nos. 1–4, pp. 340–344, Mar. 2007.
- [31] E. Blackmore, "Operation of the TRIUMF (20–500 MeV) proton irradiation facility," in *Proc. IEEE Nuclear Space Radiat. Effects Conf.*, Feb. 2000, pp. 1–5.
- [32] A. Saunders *et al.*, "Performance of the Los Alamos National Laboratory spallation-driven solid-deuterium ultra-cold neutron source," *Rev. Sci. Instrum.*, vol. 84, Feb. 2013, Art no. 013304.
- [33] C. Cazzaniga and C. D. Frost, "Progress of the scientific commissioning of a fast neutron beamline for chip irradiation," in *Proc. J. Phys., Conf.*, vol. 1021, May 2018, Art. no. 012037.
- [34] V. Agoritsas, "Secondary emission chambers for monitoring the CERN proton synchrotron ejected beams," in *Proc. Symp. Beam Intensity Meas.*, Apr. 1968, pp. 117–151.
- [35] M. Stockner, B. Dehning, C. Fabjan, G. Ferioli, and E. B. Holzer, "Measurements and simulations of ionization chamber signals in mixed radiation fields for the LHC BLM system," in *Proc. IEEE Nucl. Sci. Symp. Conf. Rec.*, Dec. 2006, pp. 1342–1345.
- [36] A. Lechner *et al.*, "Validation of energy deposition simulations for proton and heavy ion losses in the CERN large Hadron Collider," *Phys. Rev. Accel. Beams*, vol. 22, no. 7, Jul. 2019, pp. 71003–71027.
- [37] K. Roed *et al.*, "Method for measuring mixed field radiation levels relevant for SEEs at the LHC," in *Proc. 12th Eur. Conf. Radiat. Effects Compon. Syst.*, Sep. 2011, pp. 516–523.
- [38] P. G. Young and D. G. Foster, Jr., "Evaluation of the neutron and gamma-ray production cross sections for nitrogen," Los Alamos Sci. Lab., New Mexico, NM, USA, Tech. Rep., Jan. 1972, pp. 409–450, vol. 17, no. 15.
- [39] E. Bougamont *et al.*, "Neutron spectroscopy with the spherical proportional counter based on nitrogen gas," *Nucl. Instrum. Methods Phys. Res. A, Accel. Spectrom. Detect. Assoc. Equip.*, vol. 847, pp. 10–14, Mar. 2017.
- [40] M. Marzo *et al.*, "Radfet dose response in the charm mixed-field: Fluka MC simulations," *EPJ Nucl. Sci. Technol.*, vol. 3, no. 24, p. 8, Jul. 2017.